Time and temperature dependence of the scratch properties of poly(methylmethacrylate) surfaces

C. GAUTHIER, R. SCHIRRER
Institut Charles Sadron—CNRS UPR 22, 6 rue Boussingault, F-67083 Strasbourg Cedex, France
E-mail: schirrer@ics.u-strasbg.fr

Most existing models describing the scratch properties of materials take into account forces acting at the interface between the material and a grooving tip, but do not consider the stress and strain properties of the material far beneath or ahead of the tip. In the case of polymer scratches, there are no models at all which take into account the viscoelastic viscoplastic behaviour of the material. In standard indentation tests with a non moving tip, the elastic plastic boundary and the limits of the region subjected to hydrostatic pressure beneath the tip are known. These models were used to analyse the geometry of the grooves left on the surface of a viscoelastic viscoplastic body by a moving cone-shaped diamond tip having a radius of about 40 μm. A new apparatus was built to control the velocity of the tip over the range 1 to 10^4 μm/s, at several different temperatures from -10°C to 100°C. The material was a commercial grade of cast poly(methylmethacrylate) (PMMA). The normal and tangential loads and groove size were used to evaluate the dynamic hardness, which behaved like a stress and temperature activated process. Values of the activation energy and volume of the dynamic hardness and of the interfacial shear stress were in good agreement with those usually attributed to the mechanical properties of PMMA.

Symbols

a_0	contact radius
d	geometrical factor taking into account the plastic wave in scratching
E	tensile Young's modulus
E^*	Hertz contact elastic modulus
E_a	activation energy in a temperature activated process
F_n	normal load
$\dot{F}_n$	normal load rate
F_t	tangential load
H	static hardness
h	penetration depth
$\dot{h}$	penetration depth rate
h_{ep}	total penetration depth
h_e	elastic depth
h_p	plastic depth
h_{crit}	critical penetration depth
l	groove length
L_g	groove width
L_w	wave width
p_{yield}	hydrostatic yield flow or dynamic hardness
r	radius of the tip
S_w	surface of the wave cross section
S_g	surface of the groove cross section
S_τ	apparent surface area for shear contact
S_p	apparent surface area for push hydrostatic pressure contact
t	time
V_{tip}	velocity of the grooving tip
V_{rem}	volume of removed material
V_a^*	activation volume
T	temperature
k	Boltzmann constant
σ	stress
W	energy
ε	tensile strain
γ	shear strain
γ_s	interfacial shear strain
Γ	normalised volume of removed matter
θ	half apex angle of the tip
β	angle between the tip and the surface
β_0	critical value of β
μ	true friction coefficient
ν	Poisson's ratio
τ_y	shear stress at yield
τ_s	detachment shear stress at the interface
σ_y	uniaxial compression stress at yield
$\dot{\gamma}$	shear strain rate
$\overline{\sigma}_y$	equivalent mean stress
$\langle \frac{\partial \varepsilon}{\partial t} \rangle$	mean strain rate near the moving tip

1. Introduction

The surfaces of most polymers are highly sensitive to scratches, which hinders their use for high performance

optical devices. In other circumstances, polymers are used for moving mechanical parts, where friction and wear properties are important. All these situations require mechanical models to understand how the surface is damaged, models in which a moving hard tip makes a groove on the surface of a highly viscoelastic viscoplastic material. There are several ways of removing matter from a surface with a moving tip: cutting, grooving or fatigue damaging [1].

In the case of a cone-shaped moving tip, the volume V_{rem} of matter removed by plasticity was first given by [2]:

$$\frac{V_{\text{rem}}}{l} = \frac{F_{\text{n}} \cdot \tan(\pi/2 - \theta)}{\pi \cdot H} \tag{1}$$

where H is the hardness, F_{n} the normal applied load and l the path length followed by the tip. The basic assumption of this model was that all matter in the path of the moving tip is removed from the surface. On the surface of highly viscoelastic viscoplastic materials like polymers, the matter V_{rem} is in fact not removed but rather pushed in front of the tip, creating a wave ahead and on both sides. The wave dimensions depend on the geometry and speed of the tip.

One important assumption of the simple model [3] states that the tangential load F_{t} necessary to move the grooving tip subjected to a perpendicular load F_{n} is the sum of an interfacial shear yield component and a compressive "push" yield component. This is shown in Fig. 1:

$$F_{\text{t}} = \tau_{\text{s}} S_{\tau} + p_{\text{yield}} S_{\text{p}} \tag{2}$$

where τ_{s} is the interfacial shear detachment stress (nearly the true friction), S_{τ} the apparent surface area for shear contact, p_{yield} the hydrostatic pressure yield stress (dynamic scratch hardness) and S_{p} the apparent surface area for push pressure contact.

The energy W consumed to displace the volume V_{rem} may be estimated by [4]:

$$\frac{\partial W}{\partial V_{\text{rem}}} = d^2(p_{\text{yield}} + \pi \tau_{\text{s}} \tan\theta) + 2p_{\text{yield}}(1 - \Gamma)^{1/2} \tag{3}$$

where $\Gamma = (S_{\text{w}} - S_{\text{g}})/S_{\text{g}}$ is the removed matter and d is a geometrical factor taking into account the plastic wave.

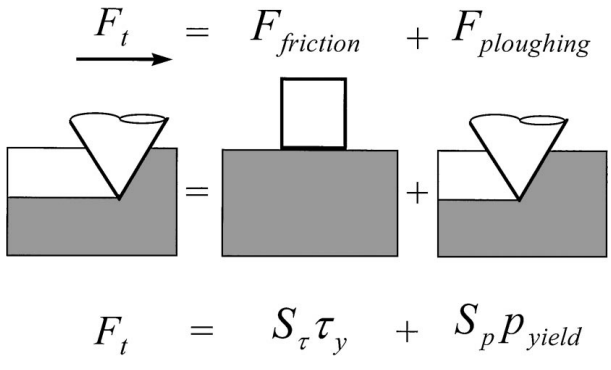

Figure 1 The model of Bowden and Tabor splits the origin of the tangential load into two terms: the friction and the ploughing.

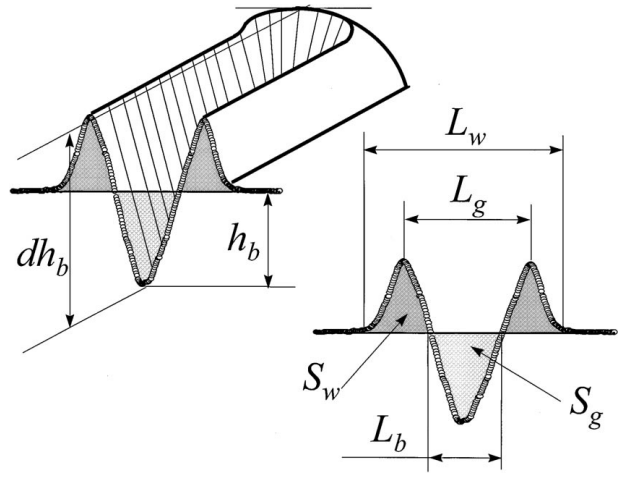

Figure 2 Cross section of a groove: dh_{b} is the height from the groove bottom to the crest of the wave ahead of the tip.

The geometry of the groove is shown in Fig. 2. The transition between the situations where matter is removed or not removed is governed by an upper value of the angle β_0, which depends on the friction coefficient μ and is given by [5]:

$$tg\left(\beta_0 - \frac{\pi}{2}\right) \approx \frac{1 - \mu^2}{2\mu} \tag{4}$$

This equation does not however take into account the wave generated ahead of the moving tip.

In the case of a spherical moving tip, the critical grooving depth h_{crit} above which matter is removed yields [6]:

$$h_{\text{crit}} = r\left[1 - \frac{\mu + 1}{[2(1 + \mu^2)]^{1/2}}\right] \tag{5}$$

where r is the radius of the sphere.

The physics of the friction coefficient μ shows that it depends on the contact time [7], on the viscoelastic behaviour of the body as described by the Johnson, Kendall and Roberts model [8] and on the yield of matter near the interface [3]. The size and shape of the zone created beneath the moving tip are not taken into account and most grooves are analysed *post mortem*. In the case of viscoelastic viscoplastic polymers, the true contact area between the moving tip and the material is somewhat difficult to predict and is therefore generally assumed to be the front half of the part of the tip in contact with the surface, as in elastic plastic bodies [9]. The dynamic scratch hardness p_{yield} is roughly twice the yield stress σ_{y} in polymers and three times the yield stress in metals [10].

The strain and stress distributions beneath the tip are best known in the case of indentation [11]. When the tip moves, the energy consumed is mainly located in two zones Fig. 3: firstly the interface, a very thin layer undergoing extremely high shear strain, a high strain rate and adhesive slipping [12], and secondly a larger and deeper volume beneath the tip where viscoplastic viscoelastic yield occurs. The latter is roughly spherical and its size is comparable to that of the groove left on

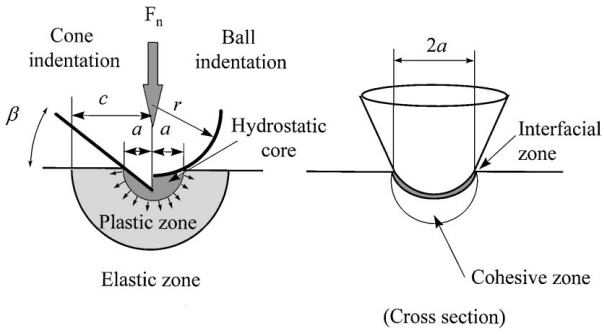

Figure 3 Left: cross section of the strain fields around the tip during indentation [11]. Right: cross section of the proposed strain fields during scratching polymers [12].

the surface. As for indentation, the following analysis will assume that the deeper volume is in turn divided into two zones: the nearest close to the tip is under pure hydrostatic pressure, while the more distant is plastically deformed. In the case of a spherical tip of radius r, the far volume undergoes large scale yielding when the load is sufficient to generate a contact radius larger than a_0 [10]:

$$a_0 \approx 40 \frac{r\sigma_y}{E^*} \tag{6}$$

Similarly, large scale yielding is caused by a cone-shaped tip when :

$$\tan\beta \approx 30 \frac{\sigma_y}{E^*} \tag{7}$$

Since the ratio $\frac{\sigma_y}{E^*}$ is of the order of 0.03 in polymers, the deep volume undergoes full yielding only for high penetration of a spherical tip. The size of the far deep volume is roughly 2 to 4 times the contact radius [10].

In this work, these concepts developed earlier for non moving tips were applied to a moving tip generating a groove. When studying a moving tip in viscoelastic viscoplastic materials like polymers, one of the most important requirements is a knowledge of the strain rate in the near and far deep volumes. Although few experimental or theoretical studies have been performed using polymers, one suggested that the local strain rate is roughly the tip velocity divided by the groove width [13]. However, in the near interfacial zone the strain rate may be several decades higher than in the far volume. Moreover, the tip generates a wave in front of it, which adds supplementary loads, and the axial loading symmetry is lost. Hence the equilibrium of a moving tip cannot be expressed as simply as in the static situation with loads acting at the surface between the tip and the scratched body. The loads applied by the body to the moving tip nevertheless indirectly reflect the surface friction and the viscoelastic viscoplastic behaviour of the near and far volumes beneath it. Therefore, a high performance apparatus was built to record the loads acting on a moving tip over wide ranges of applied load, speed and temperature. A commercial device was used to record the profiles of the grooves left on the surface. As the mechanical properties of polymers are usually thermally activated, their scratch properties were analysed by means of the usual time and temperature equations.

2. Experiments on PMMA

2.1. Experimental apparatus

Two technical approaches were employed to build the scratch apparatus. The first was based on the moving cross head of an Instron 4502 tensile machine and the whole mechanism was enclosed in the Instron environmental chamber. The second was built independently and comprised a commercial servo mechanism carrying a small temperature controlled transparent box containing only the sample and the moving tip. Control of the moving tip and recording of the load, speed and temperature were computer driven in both cases. A built-in microscope was fitted to the second apparatus to allow in situ control and measurement of the groove left on the surface. Scratching over a wide range of speeds (1 μm/s to 10^4 μm/s) and within a temperature range covering the α and β transitions of common polymers (-70 to $+120^\circ$C) are the main innovative features of these two systems. The load applied to the moving tip can be selected from 5 N to 0.05 N with better than 1% precision while the load recording system is designed to measure normal and tangential loads independently with less than 1% precision and less than 1% cross talk. The speed of the tip can be varied stepwise within a single groove in as many steps as required to explore the entire range of rate sensitivity. The moving tip is a cone-shaped diamond with a spherical point of radius 10 μm to 200 μm. Fig. 4 shows a schematic diagram of the apparatus and Fig. 5 a typical recording of speed steps and loads. Fig. 6 is an *in situ* picture taken during the scratching process.

2.2. Experimental results

All the experimental results reported below were obtained in the following manner. The clean PMMA sample was introduced into the environmental chamber and

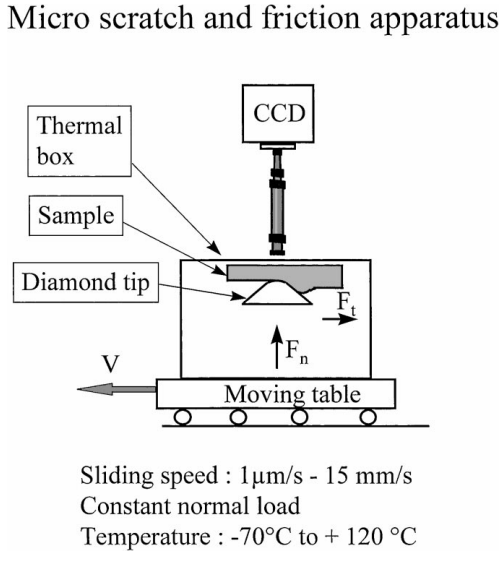

Figure 4 Experimental apparatus used in this study.

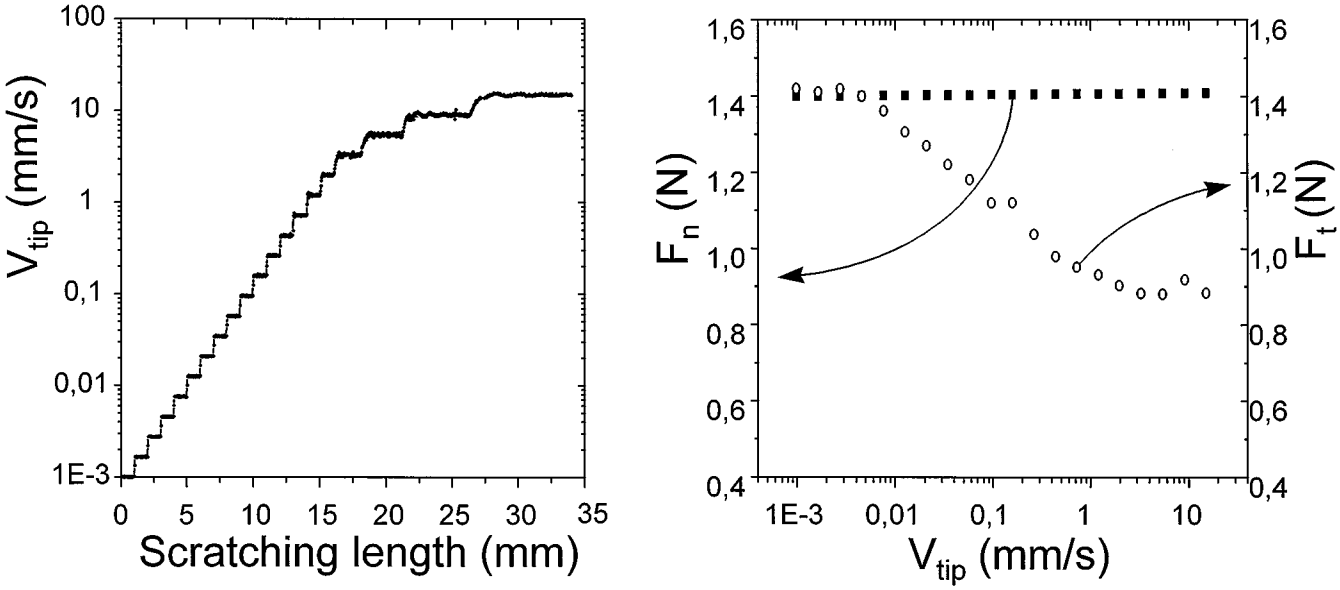

Figure 5 Scratching speed versus scratching length as imposed on the moving tip and normal and tangential loads as recorded in an experiment at 90°C.

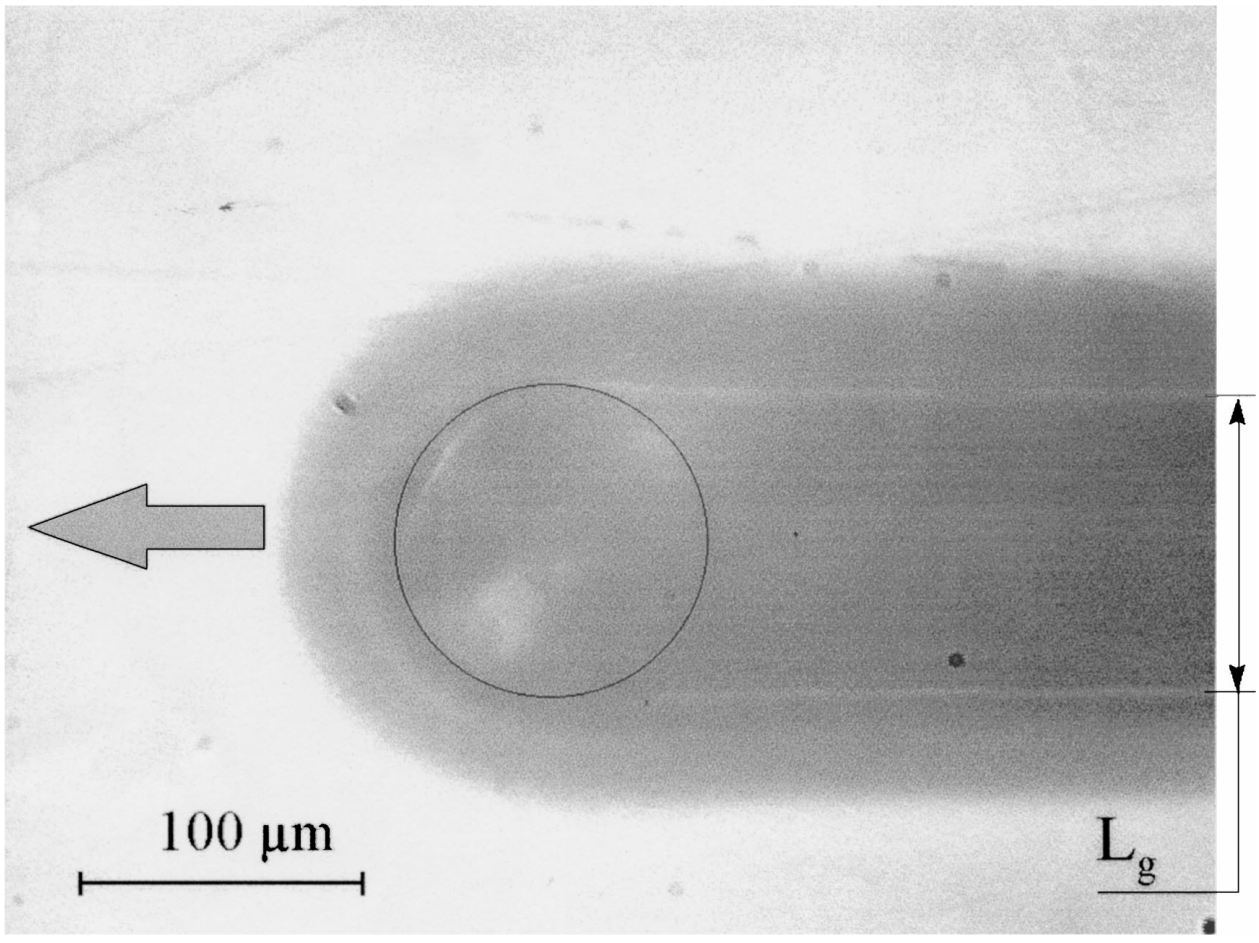

Figure 6 Live image of the moving tip at 90°C. The black circle drawn on the photograph shows the position of the diamond tip and the width L_g of the groove remains constant behind the tip.

brought to the appropriate temperature. The load at which the scratch was to be performed was then applied gently to the diamond tip. Moving of the tip was started at the slowest velocity (usually 1 μm/s) and accelerated stepwise up to the highest velocity (usually 15 mm/s). At each speed step, the tip moved over a distance of at least 1 mm so as to obtain a groove which could be easily analysed. Temperature and applied load were maintained constant throughout the entire process and the duration of one experiment (1 temperature, 20 speed

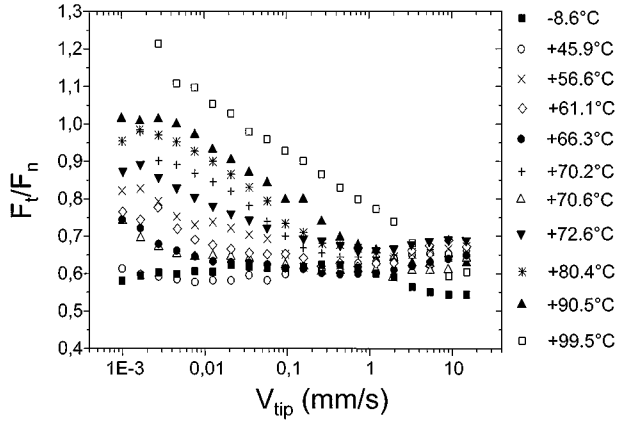

Figure 7 Apparent friction coefficient versus scratching speed. The normal load was 1.4 N and the friction appears to be a thermally activated process.

steps) was about 45 minutes. The experimental results at each temperature were the normal loads, tangential loads, *in situ* pictures and groove cross section profiles versus grooving speed.

2.2.1. Results based on the load measurements

The ratio between the tangential and normal loads in a sliding process is defined as the apparent friction coefficient, as shown in Fig. 7. In the case of a moving tip, the shape of the sliding contact surface is not planar and the friction coefficient is termed apparent. In fact, the tangential load is partly generated by true friction, but also by the geometrical effect of the viscoelastic viscoplastic wave of deformed material in front of the tip Fig. 2. Fig. 7 shows the friction coefficient obtained over 4 decades of speed and a 110 °C temperature range. The friction decreases with increasing temperature down to a limiting value of 0.6, while at each temperature this value is reached for a particular grooving speed. These variations in apparent friction with temperature and tip speed may be due either to changes in the true friction between the tip and the polymer surface, or to changes in the modulus and yield stress of the polymer affecting the wave amplitude around the moving tip.

2.2.2. Results of groove shape measurements

The size and shape of the grooves left on the surface by the moving tip were analysed at each temperature and tip speed by means of a commercial mechanical profile recorder. Fig. 8 shows that at 100°C and 5 μm/s the size of the groove may be up to 5 times greater than at -10°C and 15 mm/s. As the material is viscoelastic and viscoplastic, the cross section of the groove left on the surface is not identical to the profile of the grooving tip. The deformation of the surface, which is partially elastic, recovers partly instantaneously and partly after a short delay. Therefore, the depth of the groove is less than the penetration of the tip during its motion. Measurements of the relaxation of grooves in PMMA at room temperature indicated that relaxation is negligible after a few tenths of a second. The part recovered elastically h_e is proportional to the contact width under load and depends also on the tip shape, temperature and speed. The total groove depth h_{ep} may be split into its plastic part h_p and its elastic part h_e, as shown in Fig. 9. Such modelling in two parts has been used to describe indentations [14] and may be transposed to scratch grooves.

According to linear elasticity theory, the elastically recoverable height h_e gives:

$$h_e = F_n \frac{(1-\nu^2)}{2EL_g} \tag{8}$$

and when yielding is reached the normal load is proportional to the yield stress and contact area:

$$F_n = \alpha L_g^2 \sigma_y \tag{9}$$

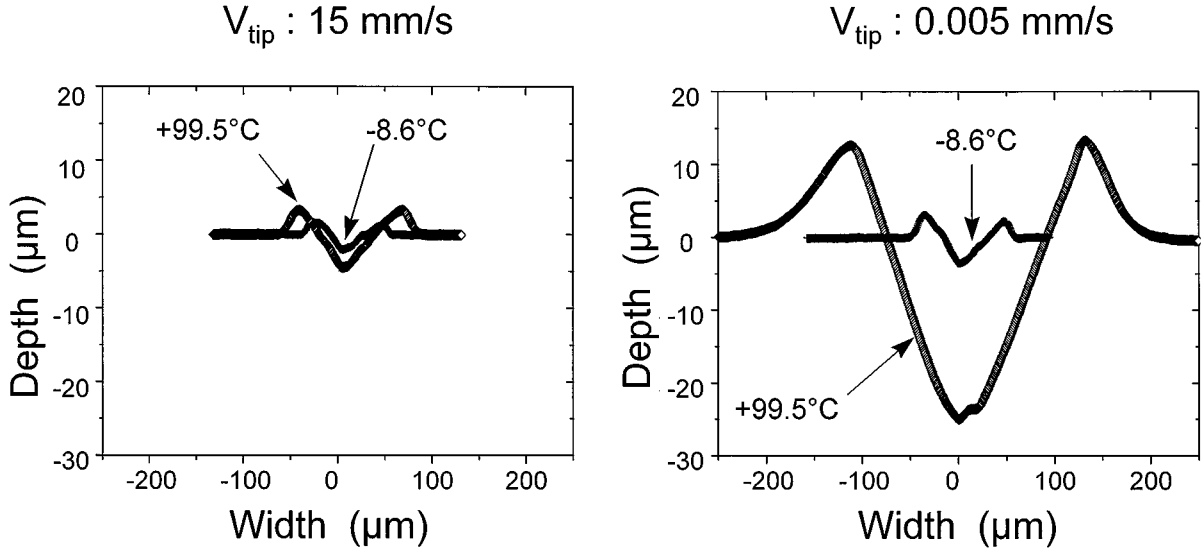

Figure 8 Groove cross sections at two temperatures and speeds: the groove size depends strongly on time and temperature while the shape is roughly homothetic.

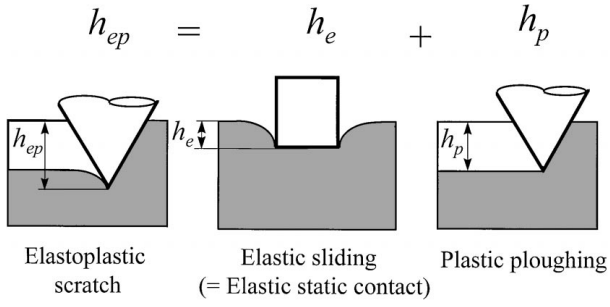

Figure 9 The model proposed in this study splits the strain mechanism around the tip into two terms: the elastic and ploughing terms.

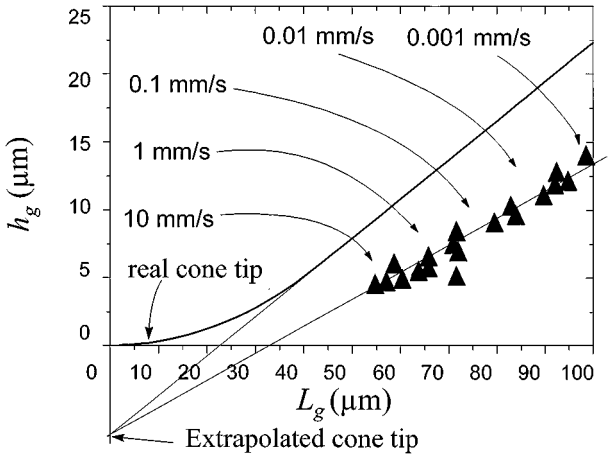

Figure 10 Depth of the groove left on the surface as a function of the tip speed at 1.4 N normal load and 60°C.

Hence h_e is proportional to the groove width L_g

$$h_e = \alpha L_g \frac{(1-\nu^2)}{2}\frac{\sigma_y}{E} \qquad (10)$$

The experimental results presented in Fig. 10 confirm this predicted linearity. Since polymers are viscoelastic and viscoplastic, these results may be equivalently obtained by varying the normal load, the temperature or the speed. This figure also shows that as the tip of the diamond is more spherical than perfectly conical, Equation 10 does not apply at very low groove depth.

2.2.3. Results of groove size and load measurements

Fig. 3 shows that beneath the penetrating tip the material is subjected to pure hydrostatic pressure. This pressure is usually called the static hardness and is defined as the ratio of the applied load to the contact area between the tip and the surface. In the case of a moving tip, the dynamic hardness may be defined in the same way, but the contact area is roughly the front half of the static penetrating area. This contact area is estimated as the half disc with a diameter equal to the groove width. In viscoelastic viscoplastic polymers, as the groove width varies strongly with time and temperature, the dynamic hardness shown in Fig. 11 varies from 100 MPa at low speed and high temperature to 800 MPa at high speed and low temperature. This result indicates that the dynamic hardness is much greater than the shear or tensile yield stress in the material.

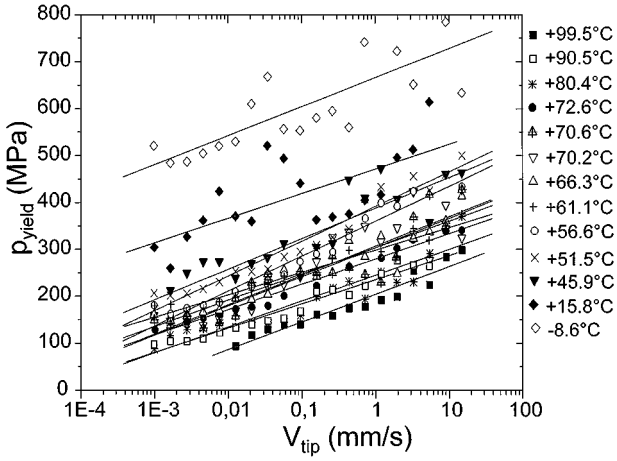

Figure 11 Dynamic hardness versus scratching speed.

3. Discussion of time and temperature dependence

3.1. Stress and temperature activated properties

3.1.1. The Arrhenius plot

Mechanical properties are usually stress and temperature activated and follow an Arrhenius process at temperatures below the glass transition. As shown in Fig. 11 the dynamic hardness varies linearly in a log(time) plot over several decades. Therefore, the mechanism may be expressed by means of an equation based on concepts similar to those used by Eyring, relating the strain rate and temperature to the material properties

$$\frac{\partial \varepsilon}{\partial t} = A\, e^{-(E_a/kT)}\, e^{(V_a^* \sigma/kT)} \qquad (11)$$

where A is a constant, E_a the activation energy, T the temperature, V_a^* the activation volume, k the Boltzmann constant, σ a material property, here the dynamic scratch hardness, the yield stress, the indentation hardness, or the interfacial detachment shear stress. The slope of σ vs. $\ln(\frac{\partial \varepsilon}{\partial t})$ at constant temperature indicates the value of V_a^*, while experiments at variable temperature provide the value of E_a. Once the activation volume and energy are known, all experiments performed at any temperature and strain rate may be plotted on a single master curve at 20°C.

3.1.2. The local strain rates beneath the moving tip

In experimental recordings, the parameter which indirectly controls the local strain rate is the speed of the grooving tip. Hence a relationship is required to connect the tip speed to the local strain rate in the material near the tip. Fig. 12 shows the different areas beneath the tip with their corresponding stress and strain states and these areas are seen to be similar to those widely accepted in the case of indentation. The relationships between tip speeds and strain rates may be obtained by examining the stress-strain history in four typical elementary volumes of the material: the volume M_1 very close to the surface which enters the interfacial area, the volume M_2 entering the hydrostatic area, the

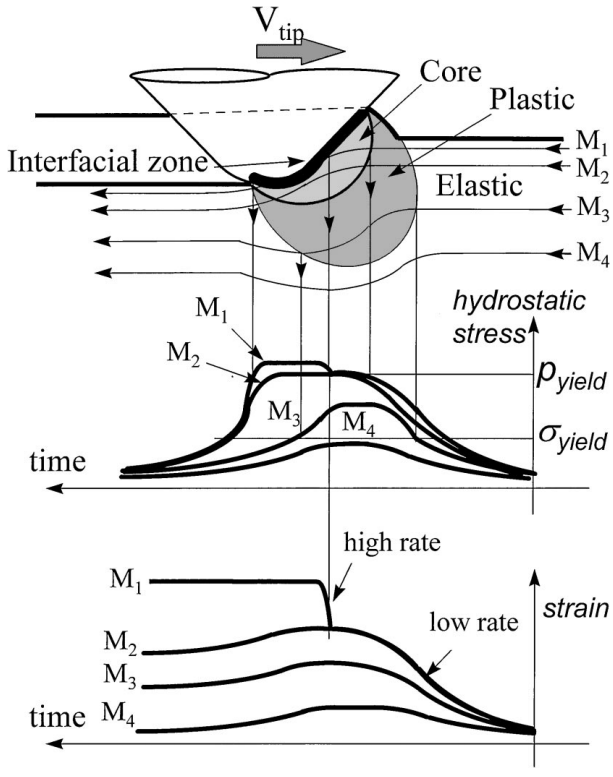

Figure 12 Stresses and strains around the tip as a function of the position of the flow line in the material.

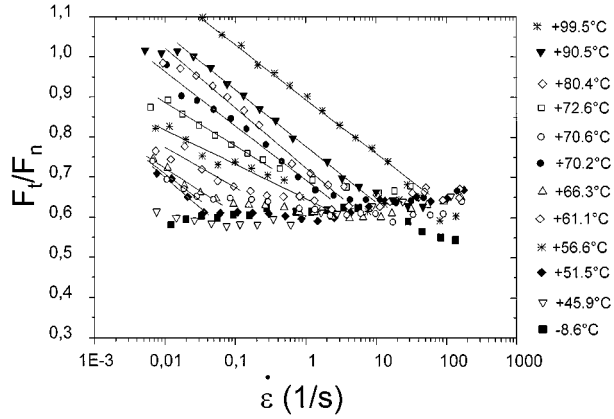

Figure 13 Apparent friction coefficient versus strain rate.

volume M_3 entering the plastic area and the volume M_4 which remains in the purely elastic area. In view of this complicated situation, it would appear to be of little worth searching for a precise quantitative connection between strain rate and tip speed. However, it is clear that two independent strain rates act respectively on M_1 and on M_2, M_3 and M_4, while the stress rates do not vary greatly among the four volumes. In addition, it would seem that two independent parameters may control the tangential load on the tip: the true local friction coefficient, which involves M_1 and has particular material properties due to the high orientation, high strain, high strain rate and low stress rate (as in laminar fluid flow), and the geometrical ploughing effect involving moderate strains and strain rates. The high strain rates and strains at the interface are unknown, but must be several decades higher than the moderate strain rates in the bulk material. As previously suggested [13] the average value of the far field moderate rate $\langle \frac{\partial \varepsilon}{\partial t} \rangle$ may be simply estimated as the tip speed divided by the groove width:

$$\left\langle \frac{\partial \varepsilon}{\partial t} \right\rangle \approx \frac{V_{\text{tip}}}{L_{\text{g}}} \tag{12}$$

where t is the time, V_{tip} the velocity of the moving tip and L_{g} the width of the groove.

3.2. The apparent friction coefficient

Fig. 7 shows the apparent friction coefficient $F_{\text{t}}/F_{\text{n}}$ as a function of tip velocity and Fig. 13 the same coefficient as a function of strain rate. In both plots, the friction coefficient exhibits a limiting low value obtained at high strain rate or low temperature. Its variations follow two regimes: the first is time and temperature dependent (high temperature, low strain rate), while the second is independent of time and temperature (low temperature, high strain rate). An Arrhenius plot Fig. 13 obtained using the regime change of this apparent friction coefficient gives values close to the secondary relaxation β of the polymer. The activation energy is of the order of 125 kJ/mol, which indicates that the transition is governed by a mechanism similar to plasticity.

Equation 2 separates the tangential load F_{t} into the part due to true friction and the part due to dynamic hardness p_{yield}. This assumption leads to the concept of an apparent friction coefficient $F_{\text{t}}/F_{\text{n}}$ depending on true friction and on dynamic scratch hardness. Fig. 11 shows that the variations of the dynamic scratch hardness follow the same time and temperature regime, similar to the first regime of the apparent friction coefficient Fig. 7, over the entire time and temperature range. In this regime, the tip penetrates deeply into the surface, increasing the geometrical plough effect which depends on the yield stress. As the strain rate increases, the yield stress also increases, the depth of penetration decreases and the plough effect becomes less important. Finally, control of the tangential load by the true friction coefficient predominates. The apparent friction coefficient is controlled by two material properties, the elastic-plastic behaviour and the true friction coefficient, and the transition between the above two regimes seems to depend on the relative levels of these two properties. This analysis shows that the apparent friction coefficient is not a material property and that its time and temperature behaviour is basically not significant.

3.3. The interfacial detachment scission

Since the apex angle of the cone-shaped tip is quite large, the second term in (2) will be neglected:

$$\tau_{\text{s}} = \frac{F_{\text{t}}}{S_{\tau}} \tag{13}$$

In Fig. 14, showing the interfacial scission stress as calculated from experimental data, the scission exhibits stress and temperature activated behaviour. As stress is fairly high beneath the moving tip (100 to 500 MPa),

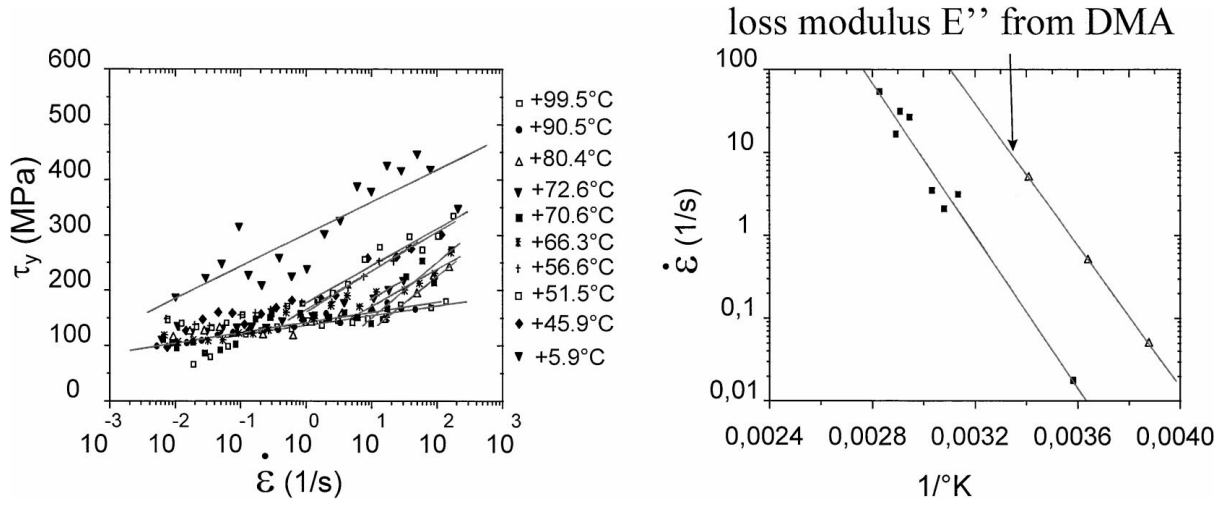

Figure 14 Scission shear stress at the interface versus strain rate. Arrhenius plots comparing the scratching process to the loss modulus from dynamic mechanical analysis (DMA).

local stress must be taken into account when calculating the activation energy. The activation volume V_a^* and true corrected activation energy E_a are derived from Fig. 14:

$$V_a^* = 0.15 \text{ nm}^3$$
$$E_a = 72 \text{ kJ/mol}$$

Fig. 15 gives the master curve for scission shear stress obtained using the above activation energy. Two different mechanisms with a transition at 10^{-1} s^{-1} and 20°C appear to control the scission and values of the scission shear stress above the transition correspond to the lower boundary value of the apparent friction F_t/F_n in Fig. 7.

3.4. The dynamic hardness

Fig. 16 shows the results of Fig. 11 for dynamic hardness plotted as a function of the strain rate calculated from the groove width. Above 50°C the grooves are smooth and the hardness can to be determined precisely. Likewise at low temperature or high strain rate they become less regular with cracks at the bottom and the precision of their profile measurement decreases strongly. Hence the plot of dynamic hardness versus strain rate displays more scatter at low temperature. The activation volume and activation energy may be calculated as for interfacial detachment shear stress:

$$V_a^* = 0.18 \text{ nm}^3$$
$$E_a = 96 \text{ kJ/mol}$$

These values agree well with those usually obtained in PMMA for mechanical properties like tensile or shear yielding, where one measures 0.2 nm^3 for V_a^* and 80 kJ/mol for E_a [15]. Fig. 17 gives the master curve for dynamic hardness reduced to a reference temperature of 20°C. The experimental procedure allows determination of the hardness over 14 decades of strain rate.

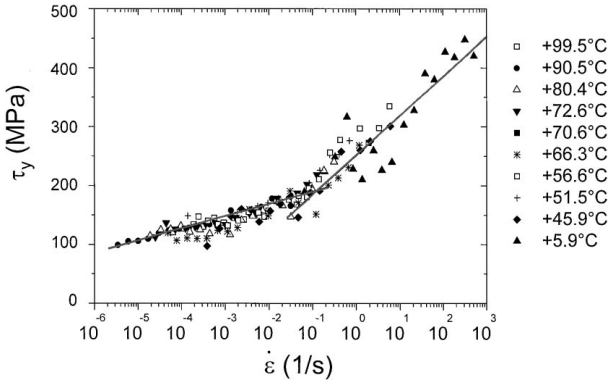

Figure 15 Master curve for the scission shear stress versus strain rate at 20°C. There are two regimes of scission stress, below and above 10^{-1} s^{-1}.

3.5. Comparison with other yielding experiments

The dynamic scratch hardness is usually considered to be twice the yield stress in polymers and three times the yield stress in metals. This result was however obtained by assuming a value of 0.5 for Poisson's ratio [10]:

$$\frac{p_{\text{yield}}}{\sigma_y} = \frac{2}{3}\left[1 + \ln\frac{1}{3}\left(\frac{E}{\sigma_{\text{yield}}}\tan\beta\right)\right] \qquad (14)$$

In polymers, where Poisson's ratio is much lower than 0.5, (14) must be rewritten as:

$$\frac{p_{\text{yield}}}{\sigma_y} = \frac{2}{3}\left[1 + \ln\left(\frac{\frac{E}{\sigma_{\text{yield}}}\tan\beta + 4(1-2\nu)}{6(1-\nu)}\right)\right] \qquad (15)$$

with for PMMA $\frac{E}{\sigma_y} \approx 35$, $\nu \approx 0.35$ and hence $\frac{p_{\text{yield}}}{\sigma_y} \approx 1.8$.

A comparison of yielding experiments in viscoelastic viscoplastic materials like polymers should take into account the strain rates in these experiments. In the case of indentation, the strain rate is [16]:

$$\frac{\partial\varepsilon}{\partial t} \approx \frac{\dot{h}}{h} \approx \frac{\dot{F}_n}{F_n} \qquad (16)$$

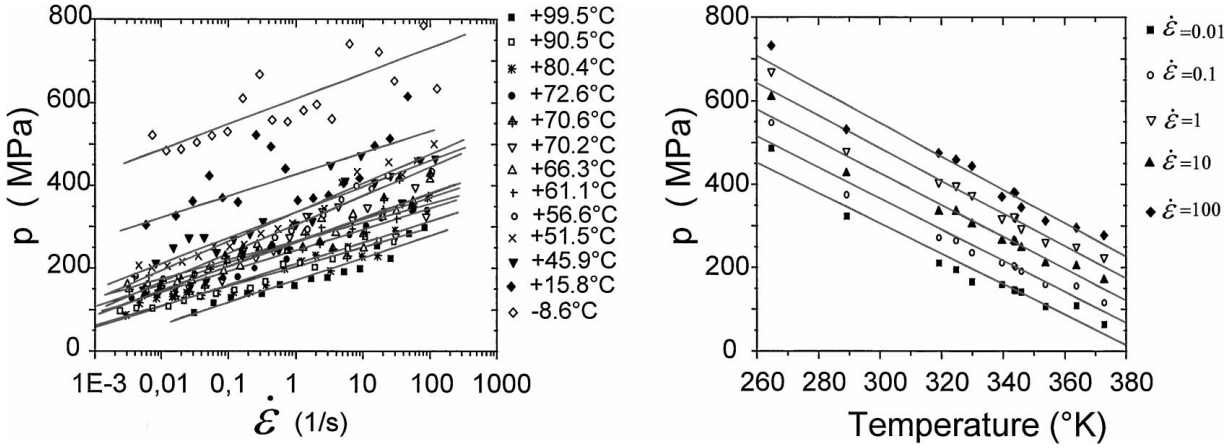

Figure 16 Left: Dynamic hardness versus strain rate. Right: Dynamic hardness versus temperature.

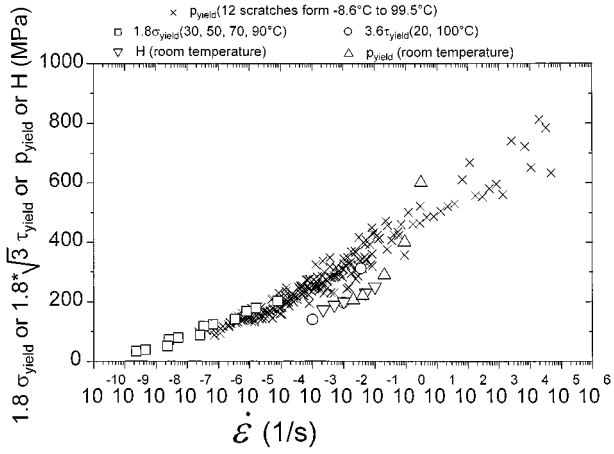

Figure 17 Master curve for the dynamic hardness from this study and the hardness and yield stresses from other studies. X: this study from -10°C to 100°C, □: compressive yield stress from 30°C to 90°C [17], Δ: nanoscratch hardness at 20°C [18], ∇: nanoindentation hardness at 20°C [18], O: Shear yield stress at 20 and 100°C [19].

while in the case of scratches the strain rate is given in (12). Therefore, the yield stress and dynamic hardness in indentation and scratching may be compared at different temperatures and strain rates. Fig. 17 compares the dynamic scratch hardness from this study with values of the compression and shear yield stress, nanoindentation hardness and dynamic scratch hardness taken from the literature. The literature values were transcribed by means of the 96 kJ/mol activation energy onto the same master curve, taking into account a factor of 1.8 from Equation 15. Shear stresses were corrected with the factor relating shear and tensile stresses:

$$\bar{\sigma}_y = \sqrt{3}\tau_y \quad \dot{\varepsilon} = \frac{2}{\sqrt{3}}\dot{\gamma} \tag{17}$$

The experimental values are listed on the same line over 14 decades of strain rate and within a temperature range of -10°C to 100°C.

However, the scratch hardness involves, in a rather complicated manner, not only the bulk compressibility but also the shear or tensile yield properties of the material. The volume beneath the tip subjected to hydrostatic pressure is in fact confined by a gradient of shear and elastic deformation, which constitutes the junction between the surface in contact with the tip and the far bulk where the material is purely elastically deformed. The way of calculating the dynamic hardness is also controversial: use of the load F_n divided by the cross sectional area of the groove assumes that the contact area between the tip and the surface is constant, which is valid for elastoplastic materials. In the case of viscoelastic materials, one may expect this contact area to vary as a function of the tip speed. Particularly at low strain rate and high temperature, the contact area could involve both the groove and the deformation wave and both the back and front faces of the tip, thus slightly increasing its value. Hence the slope of the plot of dynamic hardness versus strain rate might be lower and yield slightly lower activation volumes. The dynamic hardness as it is usually defined is therefore not an intrinsic physical property of the material, but rather a combination of several other such properties. Since all these intrinsic mechanical properties are governed by the same activation processes, the dynamic scratch hardness conserves the same activation volume and energy.

4. Conclusion

An apparatus was built to investigate the scratch properties of polymers over a temperature range of -70°C to 120°C and at scratch speeds of 1 to 10^4 μm/s. In the case of transparent polymers, the scratch was viewed with a microscope during the scratching procedure. The cross sections of the grooves left on the surface were recorded with a mechanical tactile recorder. Experiments were performed on poly(methylmethacrylate) at -10°C to 100°C and 1 to 10^4 μm/s and at loading levels of 1.4 N, using a diamond tip having a radius of 40 μm and an apex angle of 120°. The geometry of the grooves left on the surface was examined as a function of tip speed and temperature and showed that the scratch behaviour was similar to indentation behaviour. Therefore, the concepts used to analyse indentation could be adapted to scratching. The local strain rate during the scratching process was estimated as the tip speed divided by the groove width and all experimental measurements were plotted as a function of this strain rate. The scratch hardness and scission shear stress appeared to be stress

and temperature activated processes similar to other mechanical properties like elasticity or plasticity. Numerical values of the scratch hardness were consistent with those from other measurements involving plasticity such as indentation or tensile yield. It was concluded that the scratch hardness is not an independent intrinsic material property but involves other material properties associated with the flow process during scratching.

References

1. H. CZICHOS, in "Composite Materials Series, Vol. 1," edited by K. Friedrich (Elsevier, 1986) p. 1.
2. E. RABINOWICZ, "Friction and Wear of Materials," (J. Wile & Sons, 1965).
3. F. P. BOWDEN and D. TABOR, "Friction and Lubrication of Solids," (Oxford University Press, London, 1951).
4. B. LAMY, in "Microscopic Aspect of Adhesion and Lubrification," edited by J. M. Georges (Elsevier, 1982) p. 599.
5. A. J. SEDRICKS and T. O. MULHEARN, *Wear* **6** (1963) 457.
6. I. V. KRAGELSKY, "Friction and Wear," (Butterworth, London 1965).
7. P. BERTHOUD and T. BAUMBERGER, *Europhys. Lett.* **6** (1998) 617.
8. K. L. JOHNSON, K. KENDALL and A. D. ROBERTS, *Proc. R. Soc. Lond.* **A324** (1971) 301.
9. B. J. BRISCOE, P. D. EVANS, S. K. BISWAS and S. K. SINHA, *Tribology International* **2** (1996) 93.
10. K. L. JOHNSON, "Contact Mechanics," (Cambridge University Press, 1984).
11. *Idem., J. Mech. Phys. Solids* **18** (1970) 115.
12. B. J. BRISCOE, in "Composite Materials Series, Vol. 1," edited by K. Friedrich (Elsevier, 1986) p. 25.
13. B. J. BRISCOE and P. S. THOMAS, *Tribology Transactions* **38** (1995) 382.
14. J. L. LOUBET, J. M. GEORGES and G. MEILLE, in "Microindentation Techniques in Materials Science and Engineering," ASTM, STP 889, edited by P. J. Blau and B. R. Lawn (ASTM Philadelphia, 1986) p. 72.
15. J. M. LEFEBVRE and B. ESCAIG, *Polymer* **3** (1993) p. 518.
16. B. N. LUCAS, W. C. OLIVER, G. M. PHARR and J.-L. LOUBET, in "Symposium Proceedings 436, Thin Films: Stresses and Mechanical Properties VI," edited by W.-W. Gerberich, H. Gao, J.-E. Sundgren and S. P. Baker (Materials Research Society, 1997), p. 233.
17. C. BOUTON-ROCHELLE, PhD, INPL, France, 1991.
18. L. ODONI, PhD, Ecole Centrale de Lyon, France, 1999.
19. N. A. FLECK, W. J. STRONGE and J. H. LIU, *Proc. R. Soc. Lond.* **A429** (1990) p. 459.

Received 31 August
and accepted 2 November 1999